

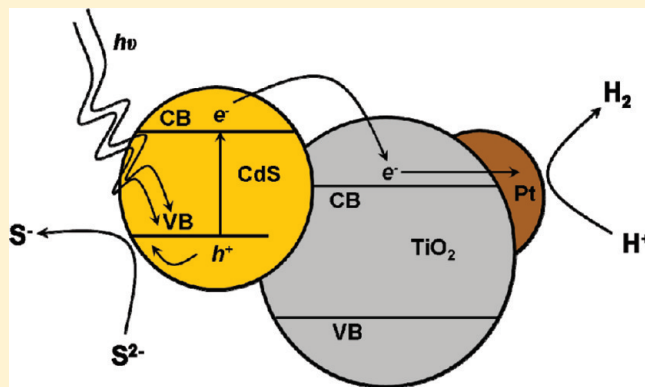
Assembly of Nanoparticles in Zeolite Y for the Photocatalytic Generation of Hydrogen from Water

Jeremy C. White and Prabir K. Dutta*

Department of Chemistry, The Ohio State University, 100 West 18th Avenue, Columbus, Ohio 43210, United States

Supporting Information

ABSTRACT: Synthesis of nanoparticles of TiO_2 , Pt, CdS, and their binary and ternary combinations were made on zeolite Y starting from molecular precursors that are ion exchanged into the zeolite. Nanoclusters of TiO_2 in the anatase form were formed from titanyl ions at low loadings of Ti (1 per 2.5 supercages). CdS (hexagonal form) and metallic Pt were formed from Cd^{2+} and $\text{Pt}(\text{NH}_3)_4^{2+}$ ion exchanged into the zeolite. Binary clusters of TiO_2 –Pt and TiO_2 –CdS were also synthesized. Electron microscopy and elemental analysis suggests colocalization of the distinct nanoparticles. Photocatalytic H_2 evolution is the strongest indicator of colocalization, since improvements in H_2 evolution rates of ~ 100 for Pt/TiO₂-zeolite over TiO₂-zeolite and ~ 18 for CdS/TiO₂-zeolite Y over CdS-zeolite Y were observed. These improvements exceed colloidal binary systems reported in the literature. However, improvements in the H_2 evolution rate of the ternary system Pt/CdS/TiO₂ was not as marked, as compared to the best colloidal ternary systems reported in the literature. A model is proposed that explains the colocalization of nanoparticles, mediated by the zeolite via a self-assembly process. This model also explains why the ternary system is not optimal; since the Pt needs to be associated only with TiO_2 for best H_2 evolution, and the zeolite-based assembly promotes a statistical colocalization of the three nanoparticles.



INTRODUCTION

Development of semiconductors suitable for efficient photoreduction of water to hydrogen is an active area of research. The most extensively studied system is TiO_2 , often combined with noble metal catalysts.^{1,2} Particular focus has been on nanosized semiconducting TiO_2 particles ($\sim 10 \text{ nm}$), which show enhanced photocatalytic activity as compared to larger size particles.¹ However, nanosized TiO_2 -based systems function only under ultraviolet light because of the wide bandgap, which limits the practical use for solar-energy-based processes.

Cadmium sulfide (CdS), with a bandgap in the visible region of radiation (2.42 eV), is another semiconductor that has also been extensively studied for photoreduction of water, including examination of various morphologies, sizes, and crystal structures.^{3–6} The limitations of CdS include low H_2 yields and photocorrosion, which can be prevented in the presence of certain electron donors (ED), the optimum being a mixture of sulfide/sulfite.^{7,8} Despite the observed improvements in stability with electron donors, it has been shown that bare CdS eventually loses its catalytic activity, even in the presence of S^{2-} .^{9,10}

In an attempt to improve the photoactivity and photostability of CdS, several strategies have been pursued. By coupling CdS with semiconductors such as TiO_2 , the coupled band structure promotes better charge separation between the electron and hole.^{3,6,8,11–13} Upon coupling with a metallic catalyst such as Pt,

hydrogen yields are enhanced.^{12,13} Such composite photocatalysts are usually prepared by colloidal synthesis. To improve photostability, incorporation into solid matrices has been explored. Incorporation of CdS into a microporous titanasilicate (ETS-4, ETS-10)^{9,10} has been reported, with the Ti–O–Ti backbone in ETS acting as a nanowire capable of accepting electrons from photoexcited CdS, and also improved the photostability of CdS.⁹

Of particular interest to the present study is the use of aluminosilicate zeolites as supports, because of their well-defined, three-dimensional microporous structure and ion-exchange properties. There have been several reports of CdS being synthesized within zeolite Y as well as hydrogen evolution studies using the $\text{S}^{2-}/\text{SO}_3^{2-}$ sacrificial electron donor system.^{14–16} CdS has also been isolated by dissolution of the zeolite matrix.¹⁷ The zeolite framework is reported to help to stabilize CdS and slow the photocorrosion.^{14,17} For incorporation of titania into zeolite Y, an ion-exchange procedure using titanyl salts followed thermal treatment has been reported.¹⁸ Though zeolite Y has been utilized for the incorporation of size-constrained CdS and TiO_2 and examined for their photocatalytic properties,^{19–23} there are no

Received: September 1, 2010

Revised: December 27, 2010

Published: February 1, 2011

reports of the two semiconductors being coupled together in zeolite Y. Added advantages of zeolites include prevention of aggregation of the nanoparticles, stabilization, as well as providing access of the solution species to the zeolite-bound particles.

In designing coupled semiconductor systems, it is essential that they be in intimate contact for efficient H₂ production.³ The proper junction structure between CdS and MoS₂ was critical in obtaining the highest hydrogen yields,²⁴ and similar effects related to particle interactions were also noted for CdS–ZnO–CdO.²⁵ Problems with the directed distribution of nanoparticles in matrices have been discussed with respect to the optimum distribution of Pt in a CdS-containing polymeric membrane.²⁶ There have been attempts at using the zeolite matrix for assembling TiO₂-based photochemical H₂ systems consisting of metal ions and heteropoly acids, but since the composite systems were prepared by impregnation on the zeolite, the host did not play a direct role in self-assembly of the composite photocatalyst.²⁷

In this paper, we examine the assembly of binary and ternary systems with nanoparticles of CdS, TiO₂, and Pt and zeolite Y as the host starting from molecular precursors. The rationale for examining the binary system of Pt/TiO₂ is the reported improvement in photocatalytic performance of TiO₂ when Pt is integrated with the TiO₂ surface.^{1,2} In the case of CdS/TiO₂, the relative positions of the band edges suggest that electrons from the conduction band of CdS can transfer to the empty conduction band of TiO₂.⁵ These materials were examined with spectroscopy, diffraction, electron microscopy, and by the rates of photochemical hydrogen production from water using sulfide/sulfite as the hole scavenger. On the basis of these studies, a model for the formation of the single, binary and ternary nanoparticle systems on the zeolite is proposed.

■ EXPERIMENTAL SECTION

Materials. Zeolite Y was purchased from Union Carbide (LZY-52, Si/Al = 2.6). Sodium hydroxide (NaOH, 98.8%) and sodium sulfite (Na₂SO₃, 98%) from Mallinckrodt were used. Ammonium titanyl oxalate (ATO) and tetraammineplatinum chloride (Pt(NH₃)₄Cl₂) were obtained from Aldrich (Milwaukee, WI, USA). Cadmium nitrate tetrahydrate (Cd(NO₃)₂·4H₂O, 99%) was from GFS Chemicals, and hydrogen sulfide (H₂S, 99%) gas was purchased from AGA Specialty Gases. High-purity methanol (MeOH, 99.99%) was from Alfa Aesar. The H₂O used in this study was purified by a Millipore ultrapure water system. These chemicals were used as received.

Synthesis. The zeolite Y (~600 nm) was cleaned by calcination at 600 °C overnight (1 °C/min) followed by cooling to 100 °C, and water-saturated air was passed over the zeolite until room temperature was reached. The zeolite was then ion exchanged using 0.1 M NaCl for 2 h, washed, filtered, and dried at 70 °C (henceforth labeled as Na-Y).

TiO₂ Zeolite Y. The inclusion of titanium dioxide into the framework of zeolite Y was carried out following reported procedures.^{18,20–22} In a typical synthesis, 3 g of Na-Y was ion exchanged for 2 h with 30 mL of 0.2 M ATO. After washing and air-drying at room temperature, the zeolite was heated at 550 °C (2 °C/min) for 5 h in the presence of flowing air. The first ATO exchanged/calcined sample will be referred to as TiO₂-Ya. For a second titanyl exchange and oxidation, the same procedure was repeated using TiO₂-Ya as the starting material, thus generating TiO₂-Yb. In the case of a third titanyl exchange/oxidation, the process was repeated once again (TiO₂-Yc).

CdS Zeolite Y. The inclusion of CdS nanoparticles into zeolite Y was carried out following reported procedures.^{14,16,19,23} Three grams of Na-Y was ion exchanged overnight in 50 mL of 0.2 M cadmium nitrate solution. The zeolite (Cd-Y) was filtered, washed, and dried at 70 °C. Cd-Y (500 mg) was then placed into a quartz tube and heated under vacuum (10⁻⁵ Torr) at 550 °C for 1 h. The dehydrated Cd-Y was then exposed to 1 atm of H₂S and allowed to react for 1 h, and the process was repeated. The cadmium sulfide containing zeolite Y (CdS-Y) was then hydrated by exposing to the ambient atmosphere for several days.

Binary Catalyst Systems. Starting with 600 mg of the TiO₂-Yb, the zeolite was ion exchanged twice for 2 h in a 0.2 M cadmium nitrate solution. After washing and drying, the zeolites were treated with H₂S as previously described. Samples generated using this protocol will be referred to as CdS/TiO₂-Yb.

CdS/TiO₂ was isolated from the zeolite matrix as follows. CdS/TiO₂-Yb (500 mg) was placed into 20 mL of 20% hydrofluoric acid (HF) in a Teflon-vessel and allowed to stir for 1 h. The solution was then centrifuged to collect the orange-yellow nanoparticles followed by several washes for neutralization.

Pt/TiO₂ zeolite photocatalysts were prepared as follows. TiO₂-Yb (200 mg) were ion-exchanged for 24 h at room temperature, using Pt(NH₃)₄Cl₂ as the platinum source (1 wt % platinum loading with respect to zeolite mass).²⁸ After washing and centrifugation, the platinum exchanged TiO₂-Y was dried overnight at 70 °C. Metallic Pt nanoparticles were formed using a thermal reduction process at 450 °C for 6 h (1 °C/min) in 5% H₂ balanced with N₂, followed by cooling in the same reaction environment (Pt/TiO₂-Yb).

Ternary Catalyst Systems. The synthetic strategy involved the deposition of Pt nanoparticles after the formation of CdS/TiO₂-Yb using the Pt(NH₃)₄Cl₂ ion-exchange process detailed above. Rather than ion exchanging the zeolite for 24 h, the zeolite in the ternary system was exchanged for only one hour prior to removing the solvent. After drying, the reduction process was carried out at 450 °C in a reducing environment to form Pt(CdS/TiO₂)-Yb.

Characterization Techniques. The diffuse reflectance absorption spectra of the zeolite-containing photocatalysts were obtained using an integrating sphere. All spectra were converted using the Kubelka–Munk transformation with zeolite Y as the reference. Crystal structure and phase composition of zeolite-bound photocatalysts were determined with either a Rigaku Geigerflex or a Bruker D8 X-ray diffractometer using nickel-filtered Cu K α (λ = 1.5405 Å) radiation. Raman spectroscopy was performed using a Renishaw–Smiths detection combined Raman–IR microprobe equipped with the 514.5-nm laser line of an argon ion laser. High-resolution electron microscopy (EM) was used to determine the particle size and crystalline structures. Transmission and scanning transmission EM were performed on either a Tecnai F20 (Philips, Holland) or Titan 3 Probe-Corrected Monochromated electron microscope (FEI Company, US) operated 260–300 kV. Both TEM instruments were capable of *in situ* elemental analysis using energy-dispersive spectroscopy (EDS). Elemental analysis of zeolite bound catalysts was performed by Galbraith Laboratories (Knoxville, Tennessee).

Photocatalytic production of H₂ was carried out in a 50-mL cylindrical Pyrex reactor for all photocatalysts. For all zeolite samples containing CdS, 50 mg of the photocatalyst was dispersed in 30 mL of water containing Na₂S (0.1 M), Na₂SO₃ (0.5 M), and NaOH (1.0 M), which serve as sacrificial reagents in the reaction. The same electrolyte solution was also used for the

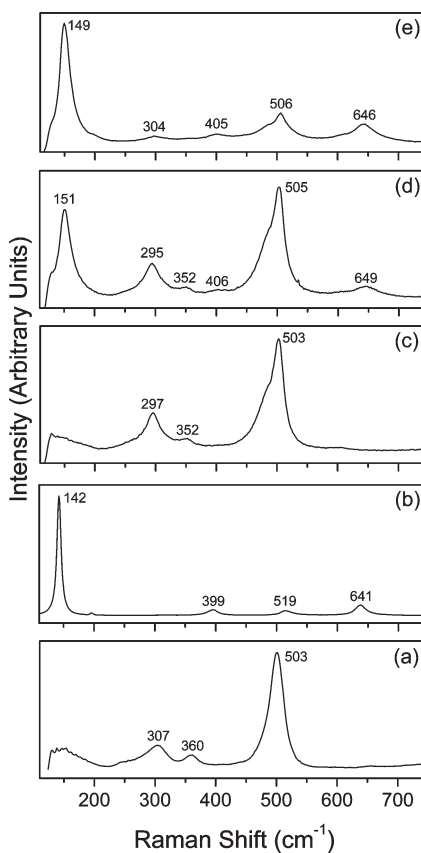


Figure 1. Raman spectra showing the formation of anatase titania in $\text{TiO}_2\text{-Y}$. (a) Zeolite Y, (b) bulk anatase TiO_2 , (c) first ATO exchange/calcination, $\text{TiO}_2\text{-Ya}$, (d) second ATO exchange/calcination, $\text{TiO}_2\text{-Yb}$, (e) third ATO exchange/calcination, $\text{TiO}_2\text{-Yc}$.

CdS/TiO_2 extracted from the zeolite using HF. All of the precipitate collected from the extraction was utilized for hydrogen evolution experiments, which was later dried into a powder for further analysis. The total weight of the catalyst (extracted CdS/TiO_2) used was 32.3 mg, and elemental analysis indicated a Cd content of 9.4 wt %. Photolysis experiments on the Pt/TiO_2 binary systems were performed in 30 mL of 33 vol % methanol in water, which has also been shown to serve as an electron donor.²

All solutions were sonicated for 5–10 min to ensure that the zeolites were well dispersed. Prior to photolysis, the solution was purged with argon for 30 min. For all experiments containing CdS , irradiation of the photocatalysts was carried out using a 200W Hg(Xe) lamp with an optical cutoff filter (Oriel 66228, $320 < \lambda < 570$), as well as a water filter (250 mW/cm^2 on the sample). For the $\text{Pt}/\text{TiO}_2\text{-Y}$ systems, no cutoff filter was used and the radiation energy was 550 mW/cm^2 . The reactions were performed with stirring. The amount of evolved H_2 was analyzed by manually injecting $50 \mu\text{L}$ of the headspace into a gas chromatograph equipped with a molecular sieve 5A column. All experimental data and reaction rates were based on irradiation times ranging from 4 to 8 h.

RESULTS

Synthesis and characterization of the single semiconductor systems of TiO_2 and CdS on the zeolite are detailed first, followed by the binary systems of CdS/TiO_2 and Pt/TiO_2 and

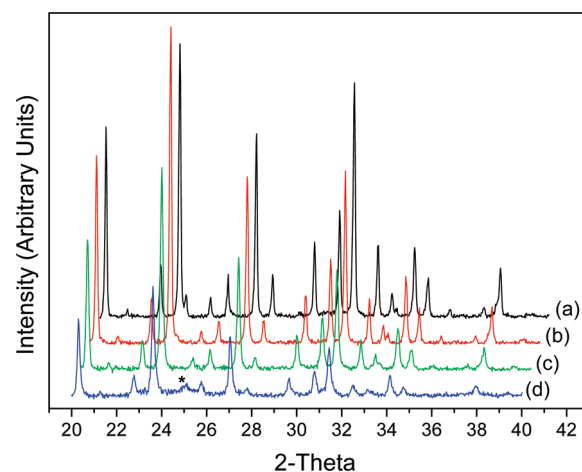


Figure 2. XRD patterns of $\text{TiO}_2\text{-Y}$ compared to untreated zeolite Y. (a) Zeolite Y, (b) first ATO exchange/calcination, $\text{TiO}_2\text{-Ya}$, (c) second ATO exchange/calcination, $\text{TiO}_2\text{-Yb}$, (d) third ATO exchange/calcination, $\text{TiO}_2\text{-Yc}$. (The asterisk corresponds to a peak from anatase.)

ternary system $\text{Pt}/\text{CdS}/\text{TiO}_2$. The hydrogen evolution with these different photocatalyst systems is then presented.

TiO₂ Zeolite Y. Ion exchange of the titanyl moiety into the zeolite was followed by thermal treatment to form titania.^{18,20–22} Ion exchange with 0.2 M ATO was done for 2 h; concentrations >0.2 M ATO caused severe zeolite framework destruction.

Figure 1a shows the Raman spectrum of zeolite Y with characteristic bands at 307, 360, and 503 cm^{-1} . For anatase TiO_2 (Figure 1b), the characteristic bands are at 142, 399, 519, and 641 cm^{-1} . Several ATO ion exchanges of Na–Y and calcination were performed. After the first exchange/calcination, Raman data in Figure 1c shows that the only change in $\text{TiO}_2\text{-Ya}$ was the broadening of the 503-cm^{-1} zeolite band when compared to parent zeolite Y in Figure 1a. After the second exchange/calcination ($\text{TiO}_2\text{-Yb}$), bands appear at 151, 406, and 649 cm^{-1} , indicating the formation of anatase TiO_2 (Figure 1d). Upon the third ion exchange and calcination, the anatase bands grow in intensity ($\text{TiO}_2\text{-Yc}$, Figure 1e). Previous Raman studies on TiO_2 zeolite have noted the presence of anatase and rutile phases,²⁹ while Figure 1 suggests only anatase formation in the present study.

The powder X-ray diffraction (XRD) of zeolite Y, along with three $\text{TiO}_2\text{-Y}$ samples, is shown in Figure 2. With increasing TiO_2 loading, there is loss in intensity of all zeolite Y peaks, and a new peak is only observed for $\text{TiO}_2\text{-Yc}$ around 25° and can be assigned to anatase (Figure 2d).²⁰ The general loss in zeolite peak intensity was not specific to certain diffraction planes but rather was proportional, thus indicating an overall loss of crystallinity in the zeolite framework. Surface area measurements reflected this destruction, as the surface area decreased from 592 to $387 \text{ m}^2/\text{g}$ from the NaY zeolite to $\text{TiO}_2\text{-Yb}$. The destruction upon titanyl exchange/calcination is consistent with previous studies.²⁰

The diffuse reflectance (DR) spectrum of $\text{TiO}_2\text{-Ya}$ does not show a clear bandgap (data not shown); for $\text{TiO}_2\text{-Yb}$ the bandgap is observed at 3.5 eV (Figure 3a), and for $\text{TiO}_2\text{-Yc}$ red shifts even further to 3.43 eV (data not shown). High-resolution TEM of $\text{TiO}_2\text{-Yb}$ in Figure 3b shows regions of crystallinity (marked with circles), with lattice fringes with a d -spacing of 0.352 nm, which is characteristic of (101) planes of anatase.³⁰ Sizes of such crystalline regions ranged from 3 to 10 nm.

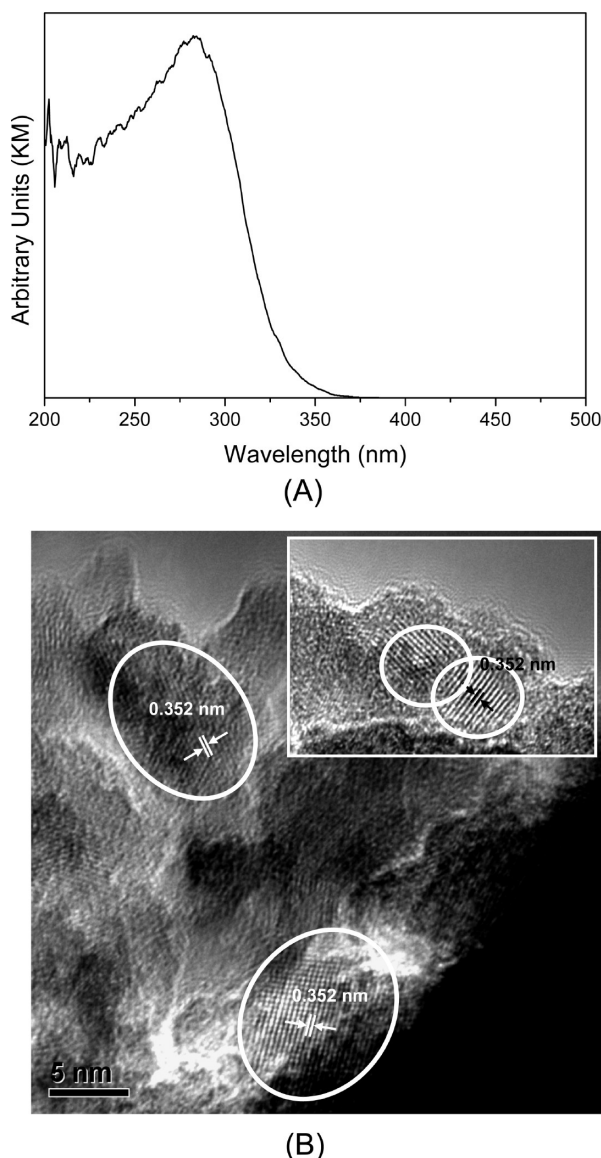


Figure 3. (A) DR absorption spectrum of $\text{TiO}_2\text{-Yb}$. (B) HR-TEM image of $\text{TiO}_2\text{-Yb}$. (Lattice spacings of 0.352 nm.)

For assembling the binary and ternary systems, we have primarily focused on $\text{TiO}_2\text{-Yb}$, since this sample is a good compromise between titania loading and zeolite destruction. The Ti loading in $\text{TiO}_2\text{-Yb}$ was measured by inductively coupled plasma optical emission spectrometry to be 0.78 wt % and corresponds to 167 μmoles Ti/g zeolite.

CdS Zeolite Y. Zeolite-bound CdS was synthesized by exposure of dehydrated Cd-Y to hydrogen sulfide gas. Powder XRD shows two broad humps between 24 and 30° and 42–46° 2 θ (Figure 4b) for CdS-Y as compared to zeolite Y (Figure 4a). Upon extraction of CdS from the zeolite, XRD of the orange-yellow powder suggests the hexagonal crystal structure, based on the seven diffraction peaks at 25.03, 26.59, 28.26, 36.85, 43.87, 48, and 52.01° 2 θ (Figure 4c, compare with the derived pattern at the bottom of Figure 4). The hexagonal structure is the more thermodynamically stable phase of CdS and is also more photocatalytically active.³¹ The diffuse reflectance spectrum of hydrated CdS-Y (Figure 5a) shows a bandgap of 2.31 eV. The Raman spectrum shows the characteristic CdS LO phonon band

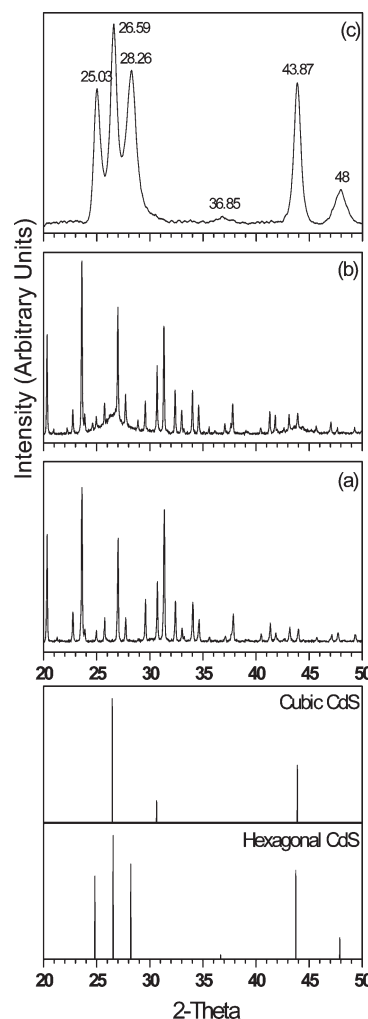


Figure 4. XRD patterns of CdS-based photocatalysts. (a) Zeolite Y, (b) CdS-Y, (c) CdS nanoparticles extracted from CdS-Y (s). Derived patterns of CdS are shown below.

at 298 cm^{-1} and its overtone at $\sim 600 \text{ cm}^{-1}$ (shown in Figure SS1 of Supporting Information).^{32,33} The high-resolution TEM shows crystalline regions, which we propose are due to CdS based on XRD and Raman spectroscopy, estimated to be $\sim 10 \text{ nm}$ in size (Figure 5b). On the basis of elemental analysis, the Cd²⁺ loading is determined to be $943 \mu\text{mol Cd}^{2+}$ per gram of zeolite for CdS-Y. Surface area of the CdS-Y was $473 \text{ m}^2/\text{g}$.

Binary Systems. Pt/ TiO_2 Zeolite Y. The deposition of Pt was carried out with $\text{TiO}_2\text{-Yb}$ by ion exchange with $\text{Pt}(\text{NH}_3)_4^{2+}$ followed by heating in a 5% H_2 stream at 550°C . Loading levels of Pt on Pt/ $\text{TiO}_2\text{-Yb}$ was 1 wt %.

XRD data shows (Figure SS2 of Supporting Information) a weak peak around $39^\circ 2\theta$ (indicated by arrow) characteristic of Pt nanoparticles.³⁴

Elemental analysis on a total of 30 randomly chosen areas in Pt/ $\text{TiO}_2\text{-Yb}$ was obtained using EDS during the TEM measurements, and the Ti/Si ratio (peak intensities of the K α lines) was estimated. These ratios are plotted in Figure SS3 of Supporting Information. Six of the sampled areas had a Ti/Si < 0.01, indicating areas containing mainly zeolitic material; seventeen had ratios between $0.01 < \text{Ti/Si} < 0.05$, and eight areas had Ti/Si ratio greater than 0.05. This suggests that only certain areas contain

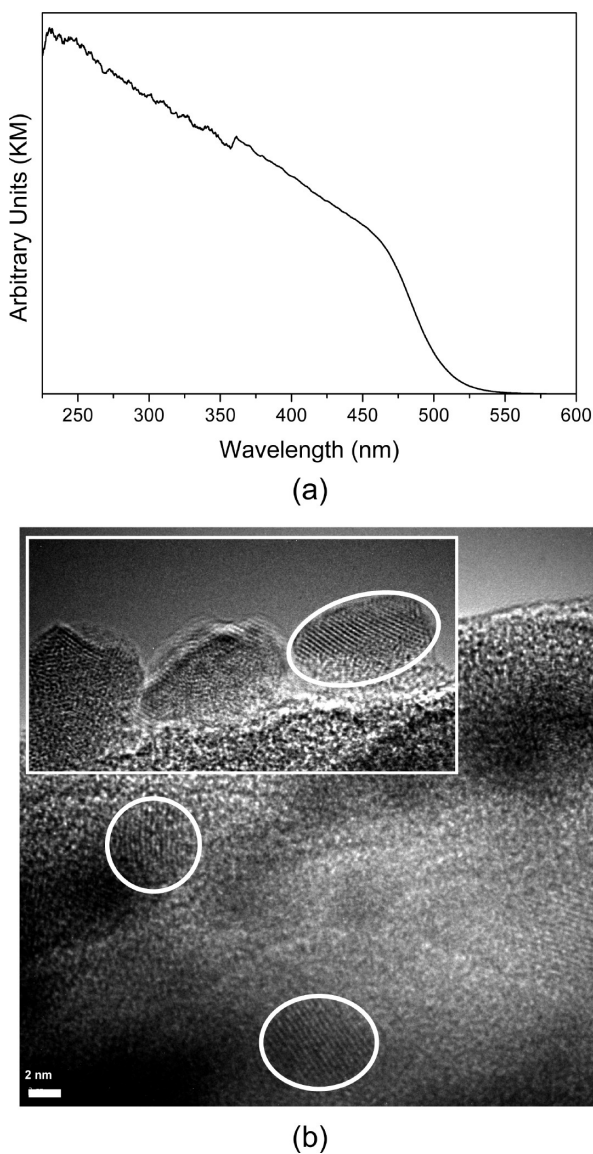


Figure 5. (A) DR absorption spectrum of CdS-Y. (B) HR-TEM image of CdS-Y.

TiO₂ particles, though the initial tianyl exchange is expected to be uniform throughout the zeolite.

By use of another sample of Pt/TiO₂-Yb, EDS was used for elemental analysis of 10 different areas of the zeolite. On the basis of the peak intensities of the L_O and K_A lines for Pt and Ti, respectively, three of the sampled areas had no Pt, while the rest had Pt (Pt/Ti ratio greater than 0.1). There were no areas found that had platinum that did not have significant titanium. Figure 6 shows the data from one of these areas, with parts a and b of Figure 6 indicating that Ti is present with no Pt, whereas parts c and d of Figure 6 indicate an area that shows both Ti and Pt presence. From the HRTEM images (Figure SS4 of Supporting Information), the size of the Pt particles was estimated to be 3–7 nm.

CdS/TiO₂ Zeolite Y. For CdS/TiO₂-Yb, there are two absorption edges at 300 and 495 nm due to CdS and TiO₂ (Figure 7A), respectively. The Raman spectrum of CdS/TiO₂-Yb is shown in Figure 7B. A total of seven Raman bands are observed, including the two characteristic phonon bands of CdS (300 and 603 cm⁻¹),

three bands for anatase TiO₂ (153, 404, and 647 cm⁻¹), and the primary Raman band of zeolite Y, which has split into two bands (464 and 506 cm⁻¹). The TEM image of CdS/TiO₂-Yb is shown in Figure 7C and has regions of crystallinity, though it is difficult to distinguish different particles. XRD of CdS/TiO₂-Yb (Figure SS5 of Supporting Information) indicates the presence of two broad diffraction peaks between 24 and 30° and 42–46° 2θ, both of which correspond well with the diffraction pattern of CdS-Y, as previously described. On the basis of elemental analysis, the Cd²⁺ loading was determined to be 455 μmol Cd²⁺ per gram of zeolite for CdS/TiO₂-Yb. The surface area of CdS/TiO₂-Yb was 286 m²/g.

Ternary Systems: Pt/CdS/TiO₂ Zeolite Y. Ternary catalyst systems consisting of Pt, CdS, and TiO₂ were assembled using the CdS/TiO₂-Yb sample by ion exchange with Pt(NH₃)₄²⁺ and treatment in hydrogen. Figure 8 shows a HRTEM image of Pt(CdS/TiO₂)-Yb, where several areas of crystallinity are noted. Figure 8b shows the elemental analysis of an area (inset), and all of the components making up the ternary system are present (Cd, S, Ti, Pt).

Photocatalytic Activity. The steady-state hydrogen evolution rates for all systems are summarized in Table 1. The H₂ evolution rate for TiO₂-Yb in 33% MeOH was determined to be 0.03 μmol/h. A H₂ evolution rate of 3.2 μmol/h was observed when Pt and TiO₂ were coupled together in Pt/TiO₂-Yb, which is an improvement by a factor of 107. The time-dependent H₂ evolution plot for the titania system are shown in Figure SS6 of Supporting Information.

Figure 9 shows the time-dependent H₂ evolution for all of the CdS-containing samples, and the rates of these H₂ evolutions are listed in Table 1. The combination of CdS and TiO₂ in the zeolite increases the rate from 0.9 μmol/h (CdS-Y) to 8.2 μmol/h, corresponding to a 9-fold increase. However, when the framework of zeolite Y is dissolved by treatment with HF and the photolysis is done with the recovered product (CdS/TiO₂(np)), the H₂ evolution rate drops by 72% to a rate of 2.3 μmol/h (when normalized to the Cd content, this drop in rate between the free and zeolite bound CdS/TiO₂ is 62%). The ternary system Pt(CdS/TiO₂)-Yb has a hydrogen production rate of 11.8 μmol/h.

DISCUSSION

Growth of metal and semiconductor clusters within zeolite has been studied extensively, and these processes often begin with ion exchange, where the ion distributes itself uniformly throughout the zeolite. However, once these ions are converted to neutral species of metal atoms or semiconductors, there is a strong tendency for large clusters to form, which cannot be accommodated within the zeolite pores and can lead to destruction of the zeolite. We observe cluster sizes of Pt, CdS, and TiO₂ in the 3–10 nm range, indicating that though these particles were all initially nucleated in the supercages (~1.3 nm), their final size exceeds the cage. We also find that the zeolite surface area decreases with introduction of these particles, indicating framework collapse, possibly around these nanoparticles. Our interest in this study is in the relative positioning of clusters: are they randomly distributed or does the zeolite promote assembly of coclusters of nanoparticles. On the basis of the results above, we address this distribution issue.

Coupling of semiconductor nanoparticles with metals and other semiconductors with appropriate band gaps has a strong

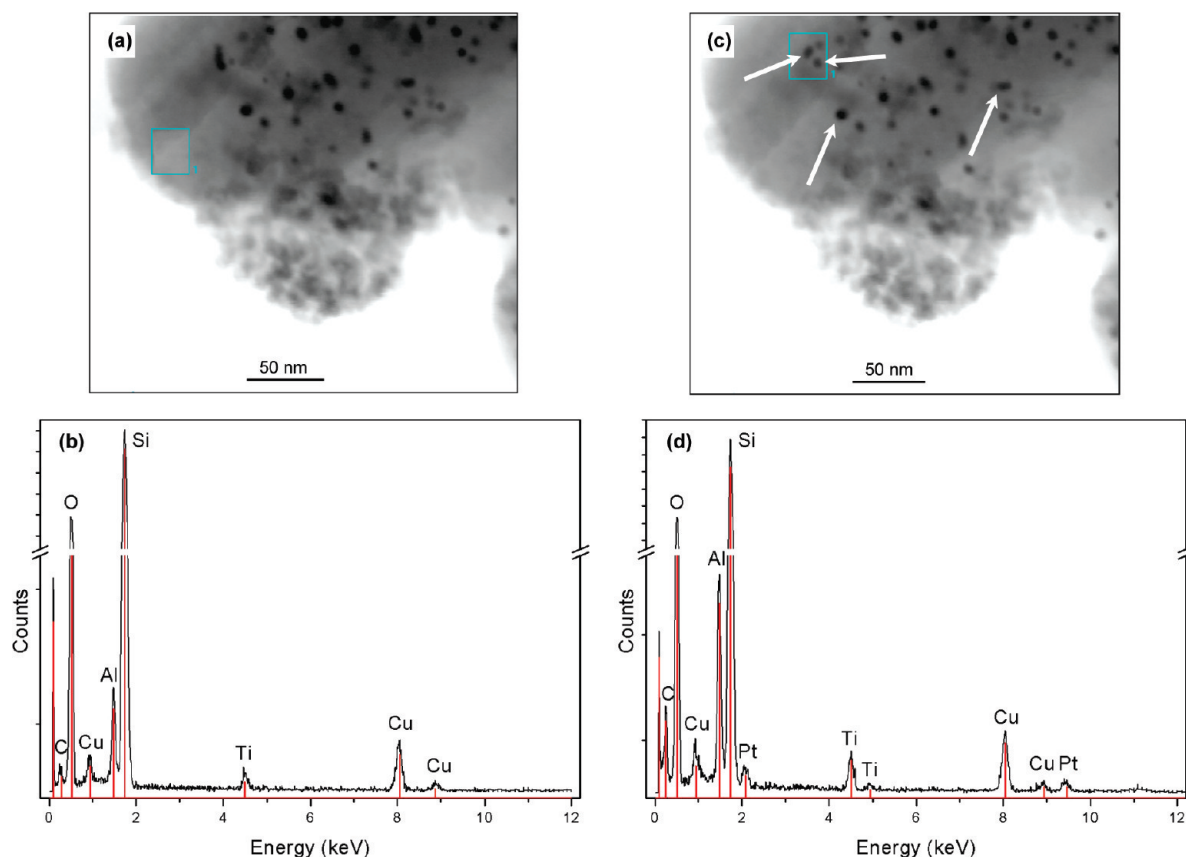


Figure 6. EDS spectra and corresponding STEM images of zeolitic areas with and without Pt nanoparticles in Pt/TiO₂–Yb. (a–b) Area containing no Pt nanoparticles, (c–d) area containing Pt nanoparticles. (White arrows indicate Pt nanoparticles.)

influence on the photocatalytic activity. For interparticle electron transfer to occur, the particles must be in close proximity. Thus, photocatalytic H₂ evolution rate is an appropriate chemical method of confirming interparticle contact. Physical measurements, such as electron microscopy, are also helpful but can be ambiguous because of the difficulty of getting elemental information from very small volumes.

Bulk elemental analysis for the TiO₂–Yb system indicates a loading of 167 μmol of Ti/g of zeolite. By consideration that there are ~450 μmol of supercages/g of zeolite, the initial titanyl ion loading level via ion exchange is low and expected to be homogeneously distributed. Upon calcination, the Raman spectrum (Figure 1d) indicates the formation of anatase. The powder diffraction for TiO₂–Yb (Figure 2c) does not show any titania peaks because of the low loading level.²⁰ The absorption spectrum (Figure 3a) and TEM (Figure 3b) indicate the formation of anatase. The titanium species must migrate during the calcination and cluster to form TiO₂. Elemental analysis (Figure S3 of Supporting Information) also suggests heterogeneous distribution of Ti once TiO₂ is formed, confirming the aggregation. Similar arguments also hold for the formation of Pt and CdS. Thus for CdS/TiO₂–Yb and Pt(CdS/TiO₂)–Yb, the Cd loading by elemental analysis is found to be 455 μmol/g of zeolite, corresponding to one Cd per supercage. Raman spectrum (Figure 7), diffraction (Figure S5 of Supporting Information), optical spectrum (Figure 7), and TEM (Figure 7) all indicate the formation of nanoparticles of CdS, indicating an aggregation process. The aggregation of CdS especially in the presence of moisture has been noted.¹⁹

Thus, it is clear that the nanoparticles are forming from the molecular species by aggregation on the zeolite. The issue for the binary (Pt/TiO₂, CdS/TiO₂) and ternary systems (Pt(CdS/TiO₂) systems is whether the nanoparticles are randomly distributed or if there is a preferential association between the particles.

We propose that the hydrogen evolution data provides insight into the arrangement of the nanoparticles. Thus, for the Pt/TiO₂ system, the rate of H₂ evolution improves by a factor of ~100 upon Pt introduction into the zeolite (0.03 to 3.2 μmol/h). A comparable study in the literature, where the Pt was produced by photoreduction on the TiO₂ zeolite, revealed that there was no significant hydrogen evolution in ethanol–water, possibly because there was no association between Pt and TiO₂.²⁰ The improvement in H₂ evolution rate of a Pt-deposited (via impregnation of chloroplatinic acid) TiO₂ (zeolite) sample with that of a TiO₂ (zeolite) sample was factor of ~1.15.²⁷ We notice a ~100 fold improvement in H₂ yield, which must arise due to colocalization of Pt and TiO₂. EM (Figure 6) and elemental analysis on Pt/TiO₂–Yb also suggests that the two particles are close. In the titanosilicate system, incorporation of Pt led to increase in H₂ evolution rate of ~10⁴, where the titanium is part of the framework and therefore is always in intimate contact with the Pt.⁹

For the binary CdS/TiO₂ system, the photoexcitation takes place into the CdS bandgap (350–550 nm). If the H₂ evolution rate is normalized to the amount of CdS, the improvement in the binary system over CdS–Y (Table 1 and 2) is a factor of 18. Also, there is a 62% loss in the catalytic activity for CdS/TiO₂ recovered after dissolving away the zeolite, suggesting that the

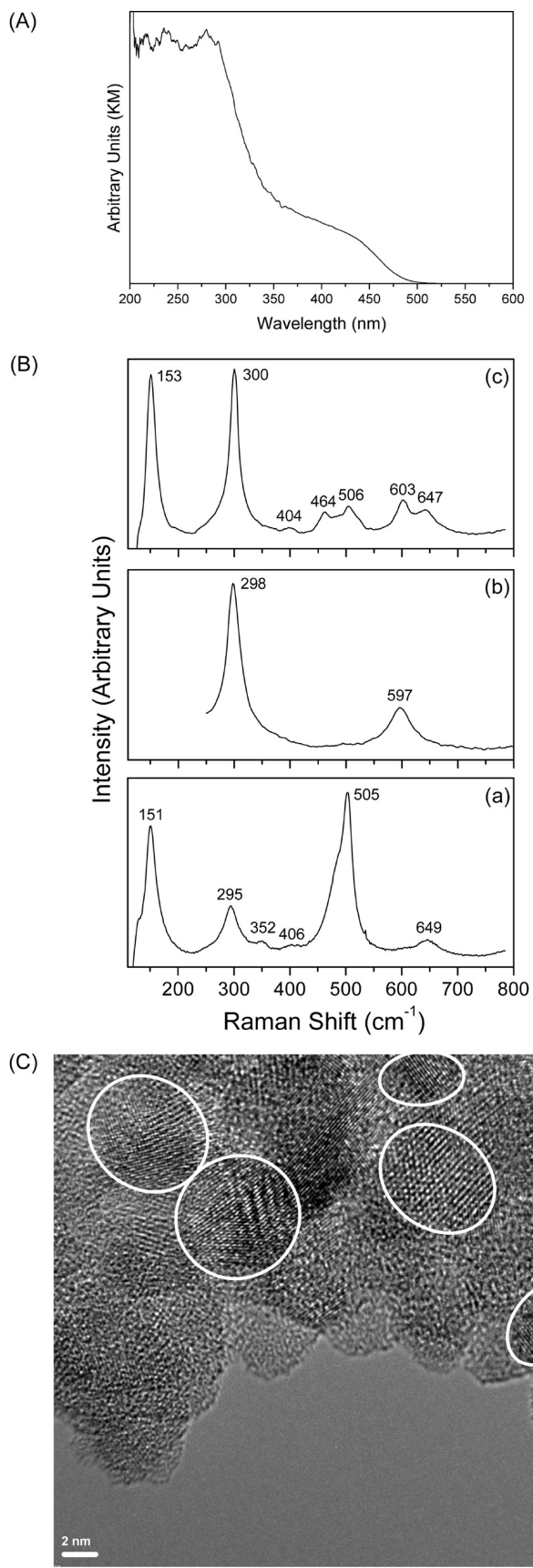


Figure 7. (A) DR absorption spectrum of $\text{CdS}/\text{TiO}_2-\text{Yb}$. (B) Raman spectra of CdS/TiO_2 binary system. (a) TiO_2-Yb , (b) extracted CdS nanoparticles, (c) $\text{CdS}/\text{TiO}_2-\text{Yb}$. (C) HR-TEM image of $\text{CdS}/\text{TiO}_2-\text{Yb}$.

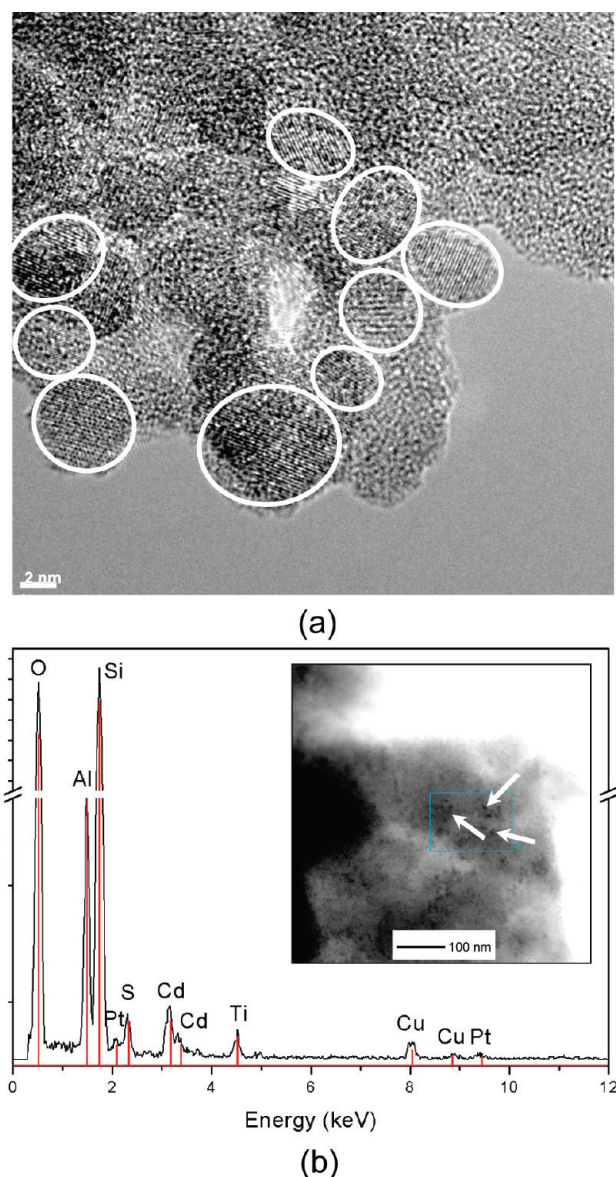


Figure 8. (a) HR-TEM image of $\text{Pt}(\text{CdS}/\text{TiO}_2)-\text{Yb}$. (b) EDS spectrum of the designated area in $\text{Pt}(\text{CdS}/\text{TiO}_2)-\text{Yb}$ and the corresponding STEM image (White arrows indicate Pt nanoparticles).

zeolite is promoting the interparticle contact. There have been several reports in the literature of CdS and CdS/TiO_2 colloidal systems. Since the amount of catalysts and photolysis conditions in these studies are very different from each other, we compare the change in the rates of H_2 evolution between the single and binary systems normalized to the CdS level, and these data are shown in Table 2. Hoffman et al. utilized colloidal dispersions of CdS and TiO_2 to demonstrate that a 3-fold increase in the normalized H_2 evolution rate.¹² Further improvement was achieved by Guan et al., in which CdS was incorporated into ETS-4, a titanosilicate zeolite.^{9,10} They showed that this combination improved the hydrogen evolution rate by 6. Jang et al. generated nanobulk composites of these materials. The coupling of these two semiconductors through colloidal synthesis led to a 13 times increase (normalized to Cd^{2+} loading) in H_2 evolution when compared to bulk CdS alone.^{8,35} Hirai et al. used surface-capped CdS nanoparticles immobilized onto TiO_2 particles.³⁶

They reported a 14-fold increase in the photocatalytic water splitting rate upon coupling these two materials. As seen from Table 2, the zeolite system with a factor of 18 improvement is better than colloidal systems, indicating that CdS and TiO₂ are in intimate contact in the zeolite. If the CdS and TiO₂ are distributed randomly then only a small fraction would have the

Table 1. Summary of the Steady-State H₂ Evolution Rates for All Zeolite-Based Photocatalysts^a

catalyst	H ₂ evolution rate ($\mu\text{mol h}^{-1}$)
TiO ₂ -Y	0.03 ^b
Pt/TiO ₂ -Yb	3.2 ± 1.6
CdS-Y	0.9 ± 0.1
CdS/TiO ₂ -Yb	8.0 ± 1.1
CdS/TiO ₂ (np)	2.3 ^b
Pt/CdS/TiO ₂ -Yb	11.8 ± 1.6

^a Samples containing CdS were irradiated using 350–550 nm light. ^b In general, the standard deviations are calculated from measurements on 2–3 independently prepared samples; however, in these two cases standard deviations were not determined.

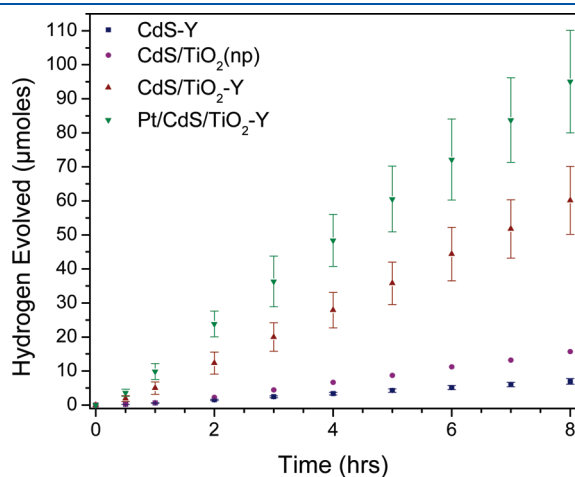


Figure 9. Time-dependent hydrogen evolution after the addition of each new material (the standard deviations were obtained from multiple independently prepared samples).

particles in contact, and the hydrogen evolution rates would not reflect the increase over colloidal systems.

For the ternary system, the addition of Pt to the CdS/TiO₂ increased the H₂ evolution rate to 11.8 $\mu\text{mol/h}$. Upon normalization with respect to the cadmium loading, this yields a 1.5 times improvement over CdS/TiO₂-Yb (Table 2). Similar results were obtained by Jang et al., in which platinization of their CdS/TiO₂ nanocomposites led to an overall rate increase of 1.5 when compared to the binary system.^{8,35} The most notable improvement in hydrogen evolution upon adding Pt to a binary system of CdS and TiO₂ was observed by Hoffman et al., in which the rate increased by a factor of 21.¹² It has been shown that the location of the Pt in the ternary system is critical in determining the H₂ efficiency and is increased by a factor of 3–30 for CdS/(Pt-TiO₂) as compared to Pt-(CdS)/TiO₂.^{3,12,13} Thus, in the ternary system, the optimum arrangement involves association of the Pt with TiO₂ rather than CdS.

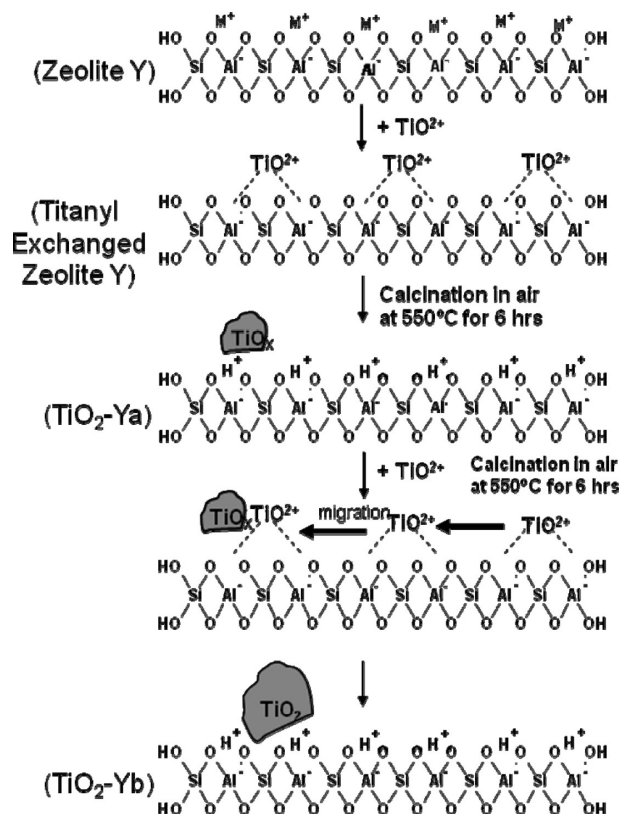
In summary, for the binary systems, we observe improvements better than the literature reports, whereas for the ternary system, that is not the case. We propose a model that can explain the colocalization of the nanoparticles on the zeolite. Chen et al. reported a detailed study of TiO₂ incorporation in zeolite and proposed a model in which TiO²⁺ species ion exchanged into the zeolite upon calcination aggregate to form TiO₂.²⁰ When a second ATO exchange is carried out to make TiO₂-Yb, ion exchange occurs throughout the zeolite. We propose that the TiO_x formed during the first calcination (TiO₂-Ya) acts as seeds and react with the migrating titanyl ions introduced in the second exchange to form larger, well-defined nanoparticles. So, even though the loading level of TiO₂ was kept low at 0.8%, TiO₂ clusters ranging from 3 to 10 nm are formed on the zeolite. This is represented in Scheme 1.

For the binary systems, upon exchanging the TiO₂-zeolite with Pt(NH₃)₄²⁺ or Cd²⁺, these ions distribute throughout the zeolite. However, upon formation of the Pt and CdS clusters within the supercages, there is a strong tendency for these particles to grow, with heat providing the impetus for Pt and moisture for CdS. Our hypothesis is that the ion-exchange sites generated close to the TiO₂ on the zeolite surface are nucleation centers for the Pt and CdS clusters that migrate from the supercages. Thus, good interparticle interaction becomes possible in the binary Pt-TiO₂ or CdS-TiO₂ clusters and is outlined in Scheme 2. As mentioned before, photoreduction or impregnation for the

Table 2. Normalized Hydrogen Evolution Rates for Our Binary and Ternary Photocatalyst Systems Compared to Previously Reported Catalyst Systems

CdS(A)		CdS/TiO ₂ (B)			Pt/CdS/TiO ₂ (C)			
catalyst	$\mu\text{mol H}_2/\mu\text{mol Cd}^{2+}\cdot\text{h}$	catalyst	$\mu\text{mol H}_2/\mu\text{mol Cd}^{2+}\cdot\text{h}$	increase (B)/(A)	$\mu\text{mol H}_2/\mu\text{mol Cd}^{2+}\cdot\text{h}$	increase (C)/(B)	increase (C)/(A)	ref
CdS nanoparticles	0.1	CdS/TiO ₂ composites	1.9	13.3	2.8	1.5	20	^{8,35}
CdS nanoparticles	1.2×10^{-2}	CdS/ETS-4(TiO ₂) composite	7.5×10^{-2}	6.3	N/A	N/A	N/A	^{9,10}
CdS nanoparticles	2.0×10^{-3}	CdS/TiO ₂ composites	5.9×10^{-3}	3.0	0.12	21.0	60	¹²
CdS nanoparticles	1.1×10^{-2}	CdS/TiO ₂ composites	0.2	13.8	N/A	N/A	N/A	³⁶
CdS Zeolite Y	1.9×10^{-2}	CdS/TiO ₂ zeolite Y composite	0.4	18.5	0.5	1.5	27	this work

Scheme 1. Proposed Mechanism for the Synthesis of $\text{TiO}_2\text{-Y}$

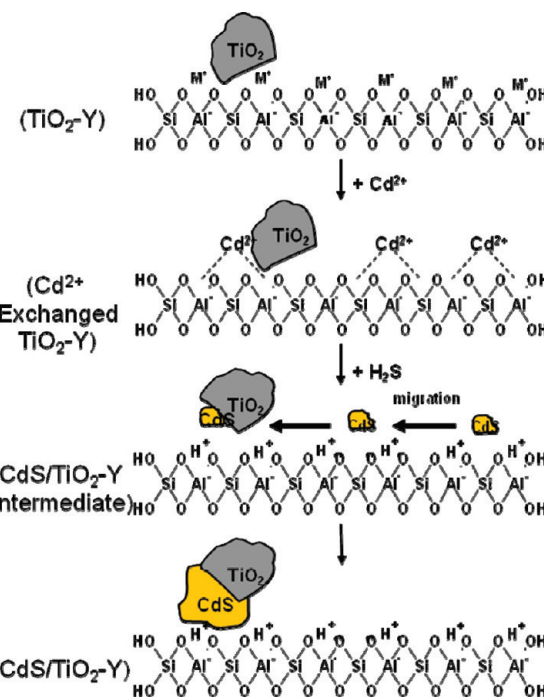


Pt/TiO₂ system did not lead to increase in rate of hydrogen production, since migration of Pt due to the heat is absent in this case.^{20,27}

It is unclear why the sites around the TiO₂ act preferentially as the initial nucleation sites and the anchoring sites for CdS or Pt. There are several possibilities. Formation of the TiO₂ leads to local destruction of the zeolite around the particle, which leads to better accommodation of the CdS/Pt units. The ion-exchange sites generated on conversion of TiO²⁺ to TiO₂ are more reactive and preferentially form the CdS and Pt. Thus, the zeolite is assisting the coassembly process of nanoparticles. In addition, the zeolite matrix also helps to support the nanoparticles and help in their stability.

Scheme 2 also explains why the ternary system did not show a significant improvement. The location of the Pt in the ternary system is critical in determining the H₂ efficiency and, for optimal reactivity, needs to be on the TiO₂.^{3,12,13} However, according to Scheme 2, the Pt particles that are being introduced to complete the ternary system can interact with CdS and/or TiO₂, and, the zeolite promoted self-assembly does not provide a route for positioning the Pt only on the TiO₂ particles. The synthesis was designed to introduce Pt after CdS and TiO₂, since sulphidation of Pt may decrease its activity. However, it would not matter if Pt was introduced before CdS, since the CdS would have no directionality to associate only with TiO₂ in the Pt/TiO₂, and CdS/Pt/TiO₂ particles could as well form. Thus, different strategies will be required to make a ternary system with a specific geometry of nanoparticles (e.g., CdS on TiO₂ with Pt associated only with TiO₂).

Scheme 2. Proposed Mechanism for the Synthesis of Binary System CdS/TiO₂-Y



ASSOCIATED CONTENT

Supporting Information. Other spectroscopic information and instrumental parameters. This material is available free of charge via the Internet at <http://pubs.acs.org>.

AUTHOR INFORMATION

Corresponding Author

*E-mail: dutta@chemistry.ohio-state.edu.

ACKNOWLEDGMENT

We acknowledge funding from the Department of Energy (DE-FG01-04ER04-20).

REFERENCES

- (1) Anpo, M.; Takeuchi, M. *J. Catal.* **2003**, *216*, 505.
- (2) Galinska, A.; Walendziewski, J. *Energy Fuels* **2005**, *19*, 1143.
- (3) Silva, L. A.; Ryu, S. Y.; Choi, J.; Choi, W.; Hoffmann, M. R. *J. Phys. Chem. C* **2008**, *112*, 12069.
- (4) Sathish, M.; Viswanath, R. P. *Catal. Today* **2007**, *129*, 421.
- (5) Sobczynski, A.; Bard, A. J.; Campion, A.; Fox, M. A.; Mallouk, T.; Webber, S. E.; White, J. M. *J. Phys. Chem.* **1987**, *91*, 3316.
- (6) Bao, N.; Shen, L.; Takata, T.; Domen, K. *Chem. Mater.* **2008**, *20*, 110.
- (7) Sabate, J.; Cervera-March, S.; Simarro, R.; Gimenez, J. *Int. J. Hydrogen Energy* **1990**, *15*, 115.
- (8) Jang, J. S.; Ji, S. M.; Bae, S. W.; Son, H. C.; Lee, J. S. *J. Photochem. Photobiol. A* **2007**, *188*, 112.
- (9) Guan, G.; Kida, T.; Kusakabe, K.; Kimura, K.; Fang, X.; Maa, T.; Abe, E.; Yoshida, A. *Chem. Phys. Lett.* **2004**, *385*, 319.
- (10) Guan, G.; Kida, T.; Kusakabe, K.; Kimura, K.; Abe, E.; Yoshida, A. *Appl. Catal., A* **2005**, *295*, 71.
- (11) Koca, A.; Sahin, M. *Int. J. Hydrogen Energy* **2002**, *27*, 363.

- (12) Park, H.; Choi, W.; Hoffmann, M. R. *J. Mater. Chem.* **2008**, *18*, 2379.
- (13) Jang, J. S.; Choi, S. H.; Kim, H. G.; Lee, J. S. *J. Phys. Chem. C.* **2008**, *112*, 17200.
- (14) Fox, M. A.; Pettit, T. L. *Langmuir* **1989**, *5*, 1056.
- (15) Stramal, R. D.; Nakamura, T.; Thomas, J. K. *J. Chem. Soc., Faraday Trans.* **1988**, *84*, 1287.
- (16) Herron, N.; Wang, Y.; Eddy, M. M.; Stucky, G. D.; Cox, D. E.; Moller, K.; Bein, T. *J. Am. Chem. Soc.* **1989**, *111*, 530.
- (17) Sathish, M.; Viswanathan, B.; Viswanath, R. P. *Int. J. Hydrogen Energy* **2006**, *31*, 891.
- (18) Liu, X.; Iu, K.; Thomas, J. K. *J. Chem. Soc. Faraday Trans.* **1993**, *89*, 1861.
- (19) Yoon, K. B.; Jeong, N. C.; Kim, H. S. *J. Phys. Chem. C.* **2007**, *111*, 10298.
- (20) Chen, H.; Matsumoto, A.; Nishimiya, N.; Tsutsumi, K. *Colloids Surf, A* **1999**, *157*, 295.
- (21) Kormann, C.; Bahnemann, D. W.; Hoffmann, M. R. *J. Phys. Chem.* **1988**, *92*, 5196.
- (22) Liu, X.; Iu, K.; Thomas, J. K. *Chem. Phys. Lett.* **1992**, *195*, 163.
- (23) Jeong, N. C.; Kim, H. S.; Yoon, K. B. *Langmuir* **2005**, *21*, 6038.
- (24) Zong, X.; Yan, H.; Wu, G.; Ma, G.; Wen, F.; Wang, L.; Li, C. *J. Am. Chem. Soc.* **2008**, *130*, 7176.
- (25) Navarro, R. M.; Del Valle, F.; Fierro, J. L. G. *Int. J. Hydrogen Energy* **2008**, *33*, 4265.
- (26) Mau, A. W.; Huang, C. B.; Kakuta, N.; Bard, A. J.; Campion, A.; Fox, M. A.; White, J. M.; Webber, S. E. *J. Am. Chem. Soc.* **1984**, *106*, 6537.
- (27) Dubey, N.; Rayalu, S. S.; Labhsetwar, N. K.; Devotta, S. *Int. J. Hydrogen Energy* **2008**, *33*, 5958.
- (28) Yang, J. C.; Dutta, P. K. *Sens. Actuators, B* **2007**, *123*, 929.
- (29) Alvaro, M.; Carbonell, E.; Atienzar, P.; Garcia, H. *ChemPhysChem* **2006**, *7*, 1996.
- (30) Li, W.; Liu, C.; Zhou, Y.; Bai, Y.; Feng, X.; Yang, Z.; Lu, L.; Lu, X.; Chan, K. Y. *J. Phys. Chem. C* **2008**, *112*, 20539.
- (31) Matsumura, M.; Furukawa, S.; Saho, Y.; Tsubomura, H. *J. Phys. Chem.* **1985**, *89*, 1327.
- (32) So, W. W.; Jang, J. S.; Rhee, Y. W.; Kim, K. J.; Moon, S. J. *J. Colloid Interface Sci.* **2001**, *237*, 136.
- (33) Sant, P. A.; Kamat, P. V. *Phys. Chem. Chem. Phys.* **2002**, *4*, 198.
- (34) Scheeren, C. W.; Machado, G.; Dupont, J.; Fichtner, P. F. P.; Texeira, S. R. *Inorg. Chem.* **2003**, *42*, 4738.
- (35) Jang, J. K.; Li, W.; Oh, S. H.; Lee, J. S. *Chem. Phys. Lett.* **2006**, *425*, 278.
- (36) Hirai, T.; Suzuki, K.; Komasawa, I. *J. Colloid Interface Sci.* **2001**, *244*, 262.